Structures of Free and Inhibited Human Secretory Phospholipase A_2 from Inflammatory Exudate

DAVID L. SCOTT, STEVEN P. WHITE, JEFFREY L. BROWNING, JOSEPH J. ROSA, MICHAEL H. GELB, PAUL B. SIGLER*

Phospholipase A_2 (PLA_2) participates in a wide range of cellular processes including inflammation and transmembrane signaling. A human nonpancreatic secretory PLA_2 (hnps-PLA_2) has been identified that is found in high concentrations in the synovial fluid of patients with rheumatoid arthritis and in the plasma of patients with septic shock. This enzyme is secreted from certain cell types in response to the proinflammatory cytokines, tumor necrosis factor or interleukin-1. The crystal structures of the calcium-bound form of this enzyme have been determined at physiological pH both in the presence [2.1 angstrom (Å) resolution] and absence (2.2 Å resolution) of a transition-state analogue. Although the critical features that suggest the chemistry of catalysis are identical to those inferred from the crystal structures of other extracellular PLA_2s, the shape of the hydrophobic channel of hnps-PLA_2 is uniquely modulated by substrate binding.

PHOSPHOLIPASES A_2 (PLA_2) HYDROlyze stereospecifically the acyl ester at the *sn-2* position of *3-sn*-phosphoglycerides. Inhibition of this reaction is of intense pharmacological interest because the release of arachidonate from the *sn-2* position of phospholipids is the rate-limiting step in the production of the eicosanoid mediators of inflammation (*1, 2*). Both intracellular and secreted forms of PLA_2 exist but their relative roles in initiating the inflammatory cascade have yet to be defined (*3*). However, the extracellular form accumulates to very high levels in diseases such as arthritis (*4, 5*) and is a potent inflammogen in several animal model (*6, 7*) and cell culture (*8*) systems.

Human nonpancreatic secretory PLA_2 (hnps-PLA_2) has been isolated from the synovial fluid of patients with rheumatoid arthritis (*9*), and its gene has been cloned and overexpressed (*10*). The cellular origin of this secretory PLA_2 is unclear, but it is identical to that isolated from platelets (*9*). In this report, we describe two crystal forms of the purified recombinant protein (Fig. 1). Both crystal forms were derived from similar conditions of pH (7.4), ionic strength (high salt), and both contain bound calcium ions (*11*). One crystal form, however, also contains a transition-state analogue (TSA) (*12*) firmly bound to each of the two representations in its asymmetric unit (hnps-PLA_2–TSA). This TSA was designed to simulate the tetrahedral intermediate formed during the hydrolysis of *L-1,2*-dioctanoyl-*sn-3*-phosphatidyl-ethanolamine and is therefore designated as diC_8(2Ph)PE. It has been used recently to study the mechanism of substrate binding and catalysis in other PLA_2's (*13–15*). Comparison of the uninhibited and inhibited crystal forms of hnps-PLA_2 permits direct identification of the stereochemical features critical to enzymatic activity and thus extends the recently published structural work on the enzyme crystallized at pH 5.5 in the absence of calcium ion (*16*).

With three notable exceptions, the sequence of hnps-PLA_2 (Fig. 2) preserves the core of residues found to be invariant or highly conserved among members of the large homologous family of extracellular PLA_2 (*17, 18*). These exceptions are the replacement of a Gln with an Asn at position 4, the replacement of a Lys with a His at position 6, and the substitution of a His for a Tyr at position 28. All three deviations appear to have significant stereochemical consequences that are described below.

The backbone conformation of the homologous core in the inhibited form of the Class II hnps-PLA_2 is, as expected, virtually superimposable on that found in the crystal structures of the pancreatic (Class I), cobra venom (Class I), and dimeric *Agkistridon piscivorus piscivorus* (Class II) enzymes (Fig. 3) (*13, 19–21*). The root-mean-square deviation of corresponding Cα atoms ranges between 0.6 and 0.7 Å. However, the conformation of the homologous core in the uninhibited crystal form of hnps-PLA_2 differs modestly from that described for other enzymes. The main contributor to this change is the amino-terminal helix, which provides side chains to the substrate-binding site and forms a substantial portion of the interfacial recognition surface (*13, 15, 22*). This nearly invariant substructure is also the focus of the structural changes that convert the pancreatic proenzyme into an enzyme that can bind to and hydrolyze aggregated substrate (*23*). In previously determined PLA_2 crystal structures (including two substrate-analogue complexes), superimposition of the respective homologous cores also superimposed the amino-terminal backbone (*13, 15, 19–22, 24–27*). In the presence of

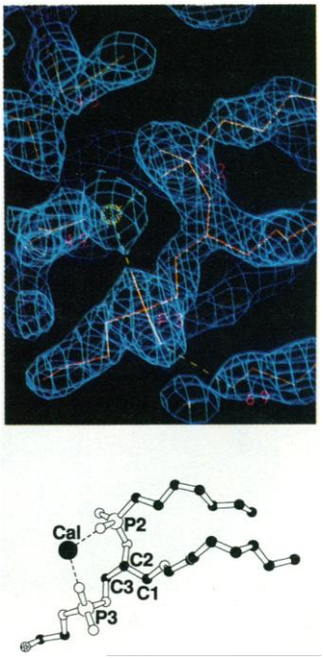

Fig. 1. Representative electron density and a corresponding schematic diagram of the transition-state analogue, *L-1-O*-octyl-*2*-heptylphosphonyl-*sn*-glycero-*3*-phosphoethanolamine. This compound was designed to emulate the tetrahedral transition state formed in the hydrolysis of dioctanoyl phosphatidylethanolamine (*12*). The electron density is a ($2F_o - F_c$) map (*31*): the *sn-2* phosphonate and the *sn-3* phosphate are labeled P2 and P3, respectively; the primary calcium ion is represented by the yellow sphere. The structures of hnps-PLA_2 and hnps-PLA_2–TSA were solved by molecular replacement (*32*) with the computer program Merlot 1.5 (*33*), modified as described (*34*). The search structure was a fusion of four existing PLA_2 structures [residues 1 to 25 = *Agkistridon piscivorus piscivorus*-D49 monomer (*35*), residues 26 to 55 = *A. p. piscivorus*–dimeric (*35*), residues 56 to 70 = notexin (*Notechis scutatus scutatus*) (*35*), and residues 71 to 133 = *Crotalus atrox*) (*24*)]. Segments were chosen for inclusion based on their sequence homology with hnps-PLA_2; nonhomologous side chains were pruned. Although all three data sets (*11*) showed strong, potential rotation function solutions, only the type I crystals yielded a convincing translation function solution. Refinement of this solution with X-PLOR (*36*) provided a new model that readily solved the translation functions of the remaining crystal forms (the structure of the type I crystal form was not further refined because of the relatively low resolution of the collected data set). X-PLOR and PROFFT (*36, 37*) refinement of the uninhibited and Type II inhibited enzyme rapidly reduced the *R* factors while improving the stereochemistries. For the uninhibited enzyme, the refinement converged with an *R* factor of 0.195 (all data from 10 to 2.2 Å) and, on average, bond lengths, interbond angle distances, and planarities deviated less than 0.015, 0.031, and 0.031 Å from ideal values, respectively. The corresponding values for the Type II inhibited form are 0.204 (all data from 10 to 2.1 Å) and 0.016, 0.035, and 0.035 Å.

D. L. Scott, S. P. White, P. B. Sigler, Department of Molecular Biophysics and Biochemistry and the Howard Hughes Medical Institute, Yale University, New Haven, CT 06511.
J. L. Browning, Department of Cell Biology and Immunology, Biogen, Inc., Cambridge, MA 02142.
J. J. Rosa, Department of Protein Chemistry, Biogen, Inc., Cambridge, MA 02142.
M. H. Gelb, Departments of Chemistry and Biochemistry, University of Washington, Seattle, WA 98195.

*To whom correspondence should be addressed.

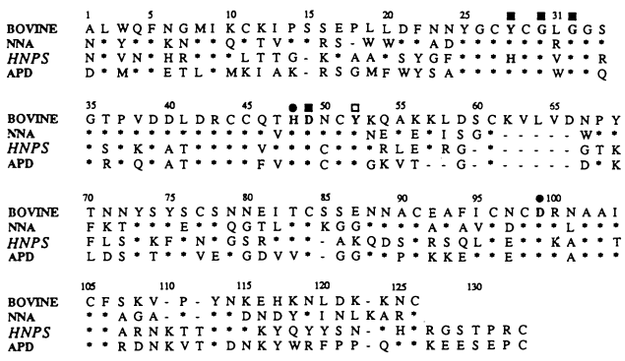

Fig. 2. Comparison of the sequence of hnps-PLA_2 with representative members of the Class I/II superfamily of extracellular PLA_2 (*17*). Top row, bovine pancreatic (Type I); second row, *Naja naja atra* venom (Type I); third row, hnps-PLA_2 (Type II); and bottom row, *Agkistridon piscivorus piscivorus* venom (Type II). The sequences are aligned according to three-dimensional structural homology (*21, 38*). Bold face indicates functionally critical residues: (●), catalytic; (■), calcium binding; and (□), the invariant supporting Tyr of the catalytic network. The sequence provided for *N. n. atra* is that inferred from the crystal structures (*13, 15*).

calcium, and at neutral pH, the eight amino-terminal residues of the uninhibited hnps-PLA_2 remain α helical but are shifted en bloc ~0.8 Å toward the primary calcium ion.

The shift of the amino-terminal helix, along with a smaller displacement of the portion of the calcium-binding loop that forms the opposing wall of the hydrophobic channel (residues 29 to 31), narrows the channel's entrance by an average of 1.2 Å from that seen in the TSA complexes (Fig. 4). The opening in the uninhibited structure is reduced to 9.9 Å as measured from the α carbon of Leu^2 to the carbonyl carbon of Gly^{30}. The relatively "closed" appearance of the channel, which was also noted in the low pH crystal structure (*16*), is caused by two of the nonconservative amino acid substitutions cited earlier, His^6 and Asn^4 (Fig. 3).

In the structure of the uninhibited form of the hnps-PLA_2, the side chain of His^6 inserts into the mouth of the hydrophobic channel instead of remaining fully exposed to bulk solvent as are the highly conserved hydrophilic side chains of other Class I and Class II enzymes. The imidazole ring lies parallel to the walls of the hydrophobic channel, and the ε2-nitrogen anchors a complex network of water molecules that extends through the hydrophobic channel and terminates at the active site. Because Asn^4 replaces the usually conserved Gln at this position, the amino-terminal helix is less well anchored and is drawn en bloc into the hydrophobic channel by the interactions of His^6. In other PLA_2 structures, the nearly invariant Gln^4 tethers the position of the amino terminus by hydrogen bonding to an adjacent peptide segment (residues 69 to 74). The shorter side chain of Asn^4 fails to provide a similar degree of stabilization and permits the helical backbone of hnps-PLA_2 to shift in response to other interactions in the local environment, such as those made with His^6. This displacement does not, however, interfere with the hydrogen-bond network linking the amino-terminal nitrogen to the active site (*21, 27*).

In the crystal structure of the TSA complex, the distal carbons of the *sn-2* acyl chain of the TSA have displaced the imidazole ring of His^6 from the hydrophobic channel (Fig. 4). The imidazole group has swung out of the hydrophobic channel to form a polarized hydrogen bond with the side chain of Glu^{17} which, in turn, is anchored to the adjacent uncovered peptide nitrogens of residues 19 and 20 at the amino terminus of a short α helix (residues 18 to 23). This amino-terminal cap forms an integral part of the recently proposed interfacial binding surface (*15*). In the presence of the TSA, the amino-terminal helix is positioned identically to that described for all other enzymes (*13, 15, 19–22, 24–27*). Thus, substrate binding enlarges the hydrophobic channel and remodels the interfacial binding surface to resemble that of other crystalline PLA_2. This finding argues against the suggestion of Wery *et al.* (*16*) that inhibitors of hnps-PLA_2 might require relatively small cross-sectional areas.

One molecule of diC_8(2Ph)PE is bound with full occupancy to each molecule of hnps-PLA_2. The electron density for the TSA is continuous except for the three distal carbons of the *sn-1* chain, which lie on the enzyme's surface and appear to be disordered. The conformation of the glycerol backbone and its substituents, as well as their relation to the catalytic residues and the primary calcium ion, is identical in each of the two representations within the asymmetric unit and corresponds precisely to that observed in the complex of diC_8(2Ph)PE with the PLA_2 from the venom of *Naja naja atra* (*13*). As predicted (*15*), the side chain of Lys^{69} forms a potentially mobile left wall for the hydrophobic channel in a manner analogous to the role played by Tyr^{69} in the elapid and pancreatic structures (*13, 22*) and Thr^{57} in the bee venom PLA_2 (*14*). This "flap" is secured into place in the TSA complex by a highly polarized hydrogen bond between the ε-amino group and the nonbridged oxygen of the *sn-3* phosphate (Fig. 1).

In the presence of the TSA, the architecture of the hydrophobic channel is similar to that observed in other PLA_2 crystal structures. There is neither structural nor biochemical evidence to suggest that this enzyme possesses any special mechanism for accommodating arachidonic acid (*all cis*-Δ5,Δ8,Δ11,Δ14-tetraeicosanoic acid) (*28*). The preference of hnps-PLA_2 for hydrolyzing lipids containing phosphatidyl-ethanolamine head groups (*9*) may result from an indirect interaction between the *sn-3* substituent and the side-chain carboxylate of Glu^{56} (4 Å away), although more complex explanations are possible, for example, those that deal with the effects of the phosphatidyl ester on the physical chemistry of the lipid aggregate.

Calcium ion is essential for PLA_2 activity

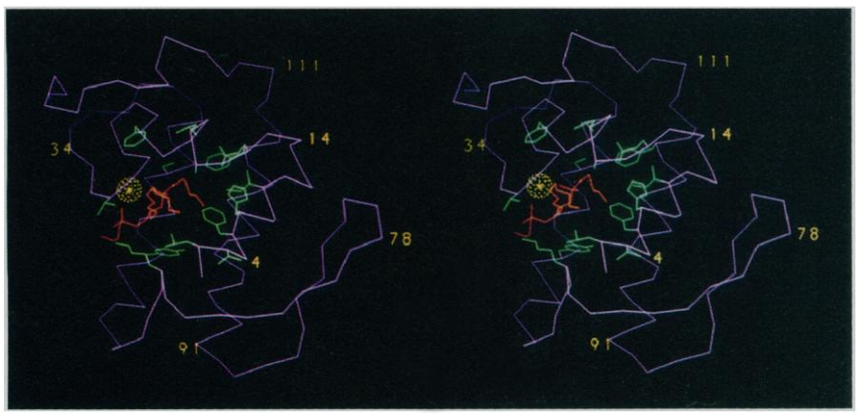

Fig. 3. Stereopair showing the Cα trace of the inhibited form of hnps-PLA_2 (magenta). The calcium ion cofactor (yellow sphere), the diC_8(2Ph)PE inhibitor (red), the side chains of the hydrophobic channel (green) [Leu^2, Phe^5, His^6, Ile^9, Ala^{19}, Val^{31}, Cys^{45}, Tyr^{52}, Lys^{69}, and Phe^{106}], and part of the interfacial binding surface (also in green) [Val^3, Glu^{17}, Leu^{20}, and Phe^{24}] are shown as they appear in the TSA complex.

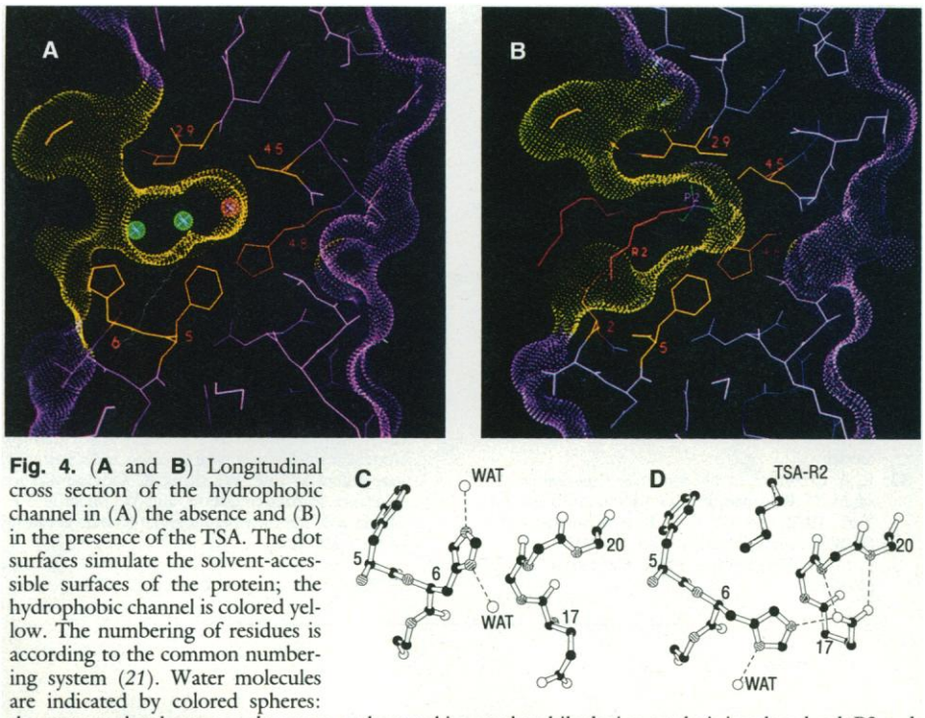

Fig. 4. (**A** and **B**) Longitudinal cross section of the hydrophobic channel in (A) the absence and (B) in the presence of the TSA. The dot surfaces simulate the solvent-accessible surfaces of the protein; the hydrophobic channel is colored yellow. The numbering of residues is according to the common numbering system (*21*). Water molecules are indicated by colored spheres: the water molecule proposed to serve as the attacking nucleophile during catalysis is colored red. P2 and R2 refer to the *sn-2* phosphonate and the *sn-2* acyl chain of the TSA, respectively. Note that the position of the side chain of His^6 in (A) appears to block access to the hydrophobic channel; in (B) His^6 is pointed out of the plane of the figure and is not shown. (**C** and **D**) Schematic representations of the interactions of His^6 in (C) the absence and (D) the presence of the TSA. These are equivalent views; water molecules are designated as WAT; the terminal segment of the *sn-2* acyl chain of the inhibitor is shown and labeled as TSA-R2. Removal of the water molecules that stabilize the imidazole group of His^6 (as well as the water molecules that stabilize the position of the side chain of Glu^{17}) by the apolar lipid environment during interfacial binding presumably promotes the formation of the hydrogen-bond pattern seen in (D).

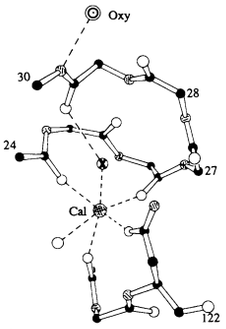

Fig. 5. Schematic representation of the secondary calcium ion's position in the crystal structure of the hnps-PLA_2–TSA complex. The charge of the secondary calcium ion (cross-hatched sphere) is potentially directed through hydrogen bonds to the peptide 29O-30N and can stabilize the oxyanion of the tetrahedral transition state (target sphere). Water molecules are represented by open spheres; the sphere marked with an X is the water molecule that serves as a "switch" since it only hydrogen bonds to the carbonyl oxygen of residue 29 in the presence of the TSA.

(*29*). Two calcium ions are present in each of the three crystallographically independent representations of hnps-PLA_2 (*30*). In each case, one calcium ion is bound to the archetypical "primary site" that is formed from the carboxylate oxygens of Asp^{49} and the carbonyl oxygens of residues 28, 30, and 32 (*15, 19*). Surprisingly, in the absence of inhibitor, the binding site for the primary calcium ion of hnps-PLA_2 lacks the two coordinated water molecules observed in other crystal structures. The TSA, however, interacts with the primary calcium ion in a manner identical to that previously reported (*13–15*). Whether this difference in the solvent cage of the primary calcium ion in the uninhibited crystal form reflects changes in bulk solvent structure (the other uninhibited calcium-containing PLA_2's were not crystallized under high-salt conditions) or reflects partial occupancy of the primary calcium ion binding site by competing sodium ions is not clear.

In both the uninhibited and inhibited forms of hnps-PLA_2, a "secondary site" derived from the amide oxygen of Asn^{122} and the backbone carbonyl oxygens of residues 24, 26, and 120, lies 8.7 Å from the primary site (Fig. 5). This six-coordinated site is located adjacent to the penta-coordinated site described for the secondary calcium ion in the *N. n. atra* TSA complex (*13*). In contrast to the *N. n. atra* system, where binding of the TSA repositions the secondary calcium ion 4.6 Å closer to the primary calcium ion, the presence of the TSA has no effect on the location of hnps-PLA_2's secondary calcium ion. Instead, only in the presence of the TSA does a water molecule forming part of the secondary calcium ion's hydration shell form a hydrogen bond to the carbonyl oxygen of residue 29, and thereby link the secondary calcium ion to the oxyanion. This is consistent with the hypothesis that the secondary calcium ion plays the role of a "supplemental electrophile" by stabilizing the oxyanion of the tetrahedral intermediate through a hyperpolarization of the 29O-30N peptide bond (*15*). The third nonconservative substitution found in hnps-PLA_2, the replacement of the highly conserved Tyr at position 28 with a His, may also affect the ability of hnps-PLA_2 to stabilize the oxyanion generated during catalysis. Although the ε2 nitrogen atom of His^{28} fulfills a structural role similar to that of Tyr^{28}'s phenolic hydroxyl group (by forming a hydrogen bond to 35O), His^{28}'s Nδ1 hydrogen bonds to one of the carboxylate oxygen atoms of Asp^{49} through an intervening water molecule. Since the carboxylate group of Asp^{49} provides two of the ligating oxygen atoms for the primary calcium ion, its interaction with His^{28} may alter the primary calcium ion's charge distribution.

REFERENCES AND NOTES

1. R. F. Irvine, *Biochem. J.* **204**, 3 (1982); F. Snyder, *Med. Res. Rev.* **5**, 107 (1985).
2. J. Chang, J. H. Musser, H. McGregor, *Biochem. Pharmacol.* **36**, 2429 (1987); B. Samuelsson, *Drug* **33**, 2 (1987); E. A. Dennis, *Biotechnology* **5**, 1294 (1987).
3. P. Vadas and W. Pruzanski, *Lab. Invest.* **55**, 391 (1986); H. Gonzalez-Buritica, M. A. Khamashta, G. R. V. Hughes, *Ann. Rheum. Dis.* **48**, 267 (1989).
4. K. Wong and E. A. Dennis, Eds., *Advances in Experimental Medical Biology* (Plenum, New York, 1990).
5. H. Kurihara, T. Nakano, N. Takasu, H. Arita, *Biochim. Biophys. Acta* **1082**, 285 (1991); H. Gonzalez-Buritica, D. M. Smith, R. A. Turner, *Ann. Rheum. Dis.* **48**, 557 (1989); J. D. Clark, N. Milona, J. L. Knopf, *Proc. Natl. Acad. Sci. U.S.A.* **87**, 7708 (1990); J. Weiss and G. Wright, in (*4*), pp. 102–114.
6. J. O. Shaw, M. F. Roberts, R. J. Ulevitch, P. Henson, E. A. Dennis, *Am. J. Pathol.* **91**, 517 (1978); W. Pruzanski, P. Vadas, V. Fornasier, *J. Invest. Dermatol.* **86**, 380 (1986); P. Vadas, W. Pruzanski, V. Fornasier, J. Kim, *Arthritis Rheum.* **29**, S37 (1986); K. R. Gans *et al.*, in (*4*), pp. 155–168; L. A. Marshall and J. Y. Chang, in (*4*), pp. 169–182; T. Nakano and H. Arita, *FEBS Lett.* **273**, 23 (1990).
7. J. S. Bomalaski, P. Lawton, J. L. Browning, *J. Immunol.* **146**, 3904 (1991).
8. B. K. Lam, C-Y. Yang, P. Y-K. Wong, in (*4*), pp. 183–191; W. Pruzanski, S. Saito, E. Stefanski, P. Vadas, *Inflammation* **15**, 127 (1991).
9. R. M. Kramer, B. Johansen, C. Hession, R. B. Pepinsky, in (*4*), pp. 35–53; R. M. Kramer *et al.*, *J. Biol. Chem.* **264**, 5768 (1989); S. Hara, I. Kudo, K. Matsuta, T. Miyamoto, K. Inoue, *J. Biochem.* **104**, 326 (1988); J. J. Seilhamer *et al.*, *ibid.* **106**, 38 (1989); A. Kanda, T. Ono, N. Yoshida, H. Tojo, M. Okamoto, *Biochem. Biophys. Res. Commun.* **163**, 42 (1989); E. Stefanski, W. Pruzanski, B. Sternby, P. Vadas, *J. Biochem.* **100**, 1297 (1986).
10. J. J. Seilhamer *et al.*, *J. Biol. Chem.* **264**, 5335 (1989); R. M. Kramer *et al.*, *ibid.*, p. 5768.
11. hnps-PLA_2 was purified from the medium of a stably transfected Chinese hamster (CHO) cell line as described (*6*). After concentration and purification with a salt gradient elution from a Sepharose FAST S resin, the protein was dialyzed into 50 mM

tris-HCl, pH 7.5, 20 mM NaCl, and 1 mM EDTA. Precipitated lipids were removed by centrifugation, and the clarified solution was passed over a Sepharose FAST Q column. The nonretained fractions were pooled and directly applied to a Sepharose FAST S column. Pure enzyme (>98%) lacking lipid contaminants was eluted from this column with 1 M NaCl and 50 mM Hepes, pH = 7.5, and dialyzed into the crystallization buffer. The crystals of the uninhibited form of hnps-PLA_2 (0.8 mm by 0.4 mm; $P6_122$; $a = b = 76.3$ Å, and $c = 90.6$ Å; one molecule in the asymmetric unit) grew in 5 days at 4°C from 10-μl droplets containing 10 mg/ml protein, 5 mM $CaCl_2$, 0.1 M tris, 2.5 M NaCl, 0.5 mM β-octyl-glucopyranoside, pH = 7.4, that were plated onto plastic cover slips and sealed over reservoirs containing 1 ml of 4.9 M NaCl, 0.1 M tris, pH = 7.4. Two different crystal forms of hnps-PLA_2–TSA were characterized. Crystals of type 1 (0.4 mm by 0.2 mm by 0.2 mm; $P6_322$; $a = b = 64.9$ Å, $c = 113.8$ Å; one molecule in the asymmetric unit) were grown in 2 weeks at room temperature from 20-μl droplets containing 10 mg/ml protein, 10 mM $CaCl_2$, 0.1 M tris, 2.0 M NaCl, pH 7.4, that were plated onto glass depression slides and sealed in boxes containing 15 ml of 4.0 M NaCl, 0.1 M tris, pH = 7.4. The crystallization of Type 2 crystals (0.5 mm by 0.5 mm by 0.4 mm; $P4_32_12$; $a = b = 76.3$ Å, $c = 115.3$ Å; two molecules in the asymmetric unit) differed from the preceeding only in that a higher NaCl concentration was used (2.25 and 4.5 M in the droplet and reservoir, respectively). Crystals of the uninhibited enzyme yielded a diffraction data set that extended to 2.2 Å resolution (R_{sym} = 0.085), Type I crystals provided data to 2.8 Å resolution (R_{sym} = 0.142), and Type II crystals diffracted to 2.1 Å resolution (R_{sym} = 0.080). All data were collected from single crystals with a dual panel San Diego Multiwire System detector; source radiation was graphite-monochromated CuKα emission from an RU-300 x-ray generator.

12. W. Yuan and M. H. Gelb, *J. Am. Chem. Soc.* **110**, 2665 (1988); W. Yuan, D. M. Quinn, P. B. Sigler, M. H. Gelb, *Biochemistry* **29**, 6082 (1990).
13. S. P. White, D. L. Scott, Z. Otwinowski, M. H. Gelb, P. B. Sigler, *Science* **250**, 1560 (1990).
14. D. L. Scott, Z. Otwinowski, M. H. Gelb, P. B. Sigler, *ibid.*, p. 1563.
15. D. L. Scott *et al.*, *ibid.*, p. 1541.
16. J.-P. Wery *et al.*, *Nature* **352**, 79 (1991).
17. The subclasses refer to a large family of homologous sequences designated by Heinrikson *et al.* [R. L. Heinrikson, E. T. Krueger, P. S. Keim, *J. Biol. Chem.* **252**, 4313 (1977)] on the basis of small differences in disulfide distribution and certain sequence segments. Class I are from mammalian pancreas and elapid venom. Class II are from crotalid and viper venom, as well as from mammalian nonpancreatic sources.
18. C. J. van den Bergh, A. J. Slotboom, H. M. Verheij, G. H. de Haas, *J. Cell. Biochem.* **39**, 379 (1989).
19. B. W. Dijkstra, K. H. Kalk, W. G. J. Hol, J. Drenth, *J. Mol. Biol.* **147**, 97 (1981).
20. A. Achari, D. L. Scott, P. B. Sigler, in preparation.
21. R. Renetseder, S. Brunie, B. W. Dijkstra, J. Drenth, P. B. Sigler, *J. Biol. Chem.* **260**, 11627 (1985). The root mean square of a collection of N values x_i is $[(\Sigma x_i^2)/N]^{1/2}$. Here x_i is the distance between the ith pair of a set of N corresponding atoms after superimposition of two molecules or molecular segments. The program used was originally developed by A. Lesk.
22. M. M. G. M. Thunnissen *et al.*, *Nature* **347**, 689 (1990).
23. J. P. Abita, M. Lazdunski, P. P. M. Bonsen, W. A. Pieterson, G. H. de Haas, *Eur. J. Biochem.* **30**, 37 (1972); M. A. Pieterson, J. J. Volwerk, G. H. de Haas, *Biochemistry* **13**, 1455 (1974).
24. S. Brunie, J. Bolin, D. Gerwirth, P. B. Sigler, *J. Biol. Chem.* **260**, 9742 (1985).
25. B. W. Dijkstra, R. Renetseder, K. H. Kalk, W. G. J. Hol, J. Drenth, *J. Mol. Biol.* **168**, 163 (1983).
26. D. R. Holland *et al.*, *J. Biol. Chem.* **265**, 17649 (1990).
27. A. Achari *et al.*, *Cold Spring Harbor Symp. Quant. Biol.* **52**, 441 (1987).
28. J. L. Browning, unpublished observations; C. G. Schalkwijk, F. Maerki, H. Van den Bosch, *Biochim. Biophys. Acta* **1044**, 139 (1990).
29. M. Waite, *The Phospholipases*, vol. 5 of *Handbook of Lipid Research* (Plenum, New York, 1987).
30. Calcium ions are identified by the refinement assigning a compact density of 18 electrons to the site with a temperature factor consistent with those of the surrounding atoms. Attempts to assign a water molecule to the same density caused the refinement to simulate an even more compact higher density by imposing a physically unrealistic temperature factor. There is no way to confidently distinguish a calcium ion from the isoelectronic potassium ion by x-ray crystallography; however, no potassium salts were used in the preparation or purification of the proteins, $diC_8(2Ph)PE$, or any of the crystal-stabilizing supernatant solutions.
31. The coefficients of the Fourier sum are $(2F_o - F_c)\exp(i\phi_c)$, where F_o is the observed amplitude and F_c and ϕ_c are the amplitude and phase, respectively, of the structure factors calculated from the refined model.
32. R. A. Crowther, in *The Molecular Replacement Method*, M. G. Rossman, Ed. (Gordon and Breach, New York, 1972), pp. 173–178; R. A. Crowther and D. M. Blow, *Acta Crystallogr.* **23**, 544 (1967).
33. P. M. D. Fitzgerald, *J. Appl. Crystallogr.* **21**, 273 (1988).
34. Z. Otwinowski *et al.*, *Nature* **335**, 321 (1988).
35. D. L. Scott *et al.*, manuscripts in preparation.
36. A. T. Brünger, J. Kuriyan, M. Karplus, *Science* **235**, 458 (1987).
37. W. A. Hendrickson and J. H. Konnert, *Biomolecular Structure, Function, Conformation and Evolution*, R. Srinivasan, Ed. (Pergamon, Oxford, 1981), vol. 1, pp. 43–57; B. C. Finzel, *J. Appl. Crystallogr.* **20**, 53 (1987).
38. Abbreviations for the amino acid residues are: A, Ala; C, Cys; D, Asp; E, Glu; F, Phe; G, Gly; H, His; I, Ile; K, Lys; L, Leu; M, Met; N, Asn; P, Pro; Q, Gln; R, Arg; S, Ser; T, Thr; V, Val; W, Trp; and Y, Tyr.
39. The coordinates will be deposited in the Brookhaven Protein Data Bank. The research at Yale was supported by NIH grant no. GM22324 and by the Howard Hughes Medical Institute; the research at the University of Washington was supported by NIH grant no. HL36235. S.P.W. was a fellow of the Arthritis Foundation, and D.L.S. was a graduate student at the University of Chicago and a postgraduate fellow at Yale. We thank Z. Otwinowski for assistance in data collection, and W. Meier and K. Miatkowski for their help with large-scale culturing of the CHO line.

13 June 1991; accepted 30 August 1991

Induction of Type I Diabetes by Kilham's Rat Virus in Diabetes-Resistant BB/Wor Rats

D. L. GUBERSKI, V. A. THOMAS, W. R. SHEK, A. A. LIKE,* E. S. HANDLER, A. A. ROSSINI, J. E. WALLACE, R. M. WELSH

Type I diabetes mellitus is an autoimmune disease resulting from the interaction of genetic and environmental factors. A virus that was identified serologically as Kilham's rat virus (KRV) was isolated from a spontaneously diabetic rat and reproducibly induced diabetes in naive diabetes-resistant (DR) BB/Wor rats. Viral antigen was not identified in pancreatic islet cells, and β cell cytolysis was not observed until after the appearance of lymphocytic insulitis. KRV did not induce diabetes in major histocompatibility complex–concordant and discordant non-BB rats and did not accelerate diabetes in diabetes-prone BB/Wor rats unless the rats had been reconstituted with DR spleen cells. This model of diabetes may provide insight regarding the interagation of viruses and autoimmune disease.

VIRAL INFECTIONS HAVE BEEN considered possible etiologic agents responsible for human type I diabetes with the coxsackie (*1, 2*) and rubella (*3*) viruses as the most likely candidates. Proposed mechanisms of action include virus-induced modification of β cell antigens, molecular mimicry, direct lysis of β cells, and virus-induced functional changes in effector or regulatory lymphocytes (*4, 5*). All experimental models of virus-induced diabetes so far involve viral infection or transfection of β cells, and there has been no direct demonstration that viruses induce diabetes in experimental animals without extensive β cell infection or lysis (*4–6*). We report here a model for the study of virus-induced diabetes in rats with a discrete genetic background.

The BB/Wor rat develops spontaneous, autoimmune diabetes mellitus and is considered an animal model of human type I insulin-dependent diabetes mellitus. Diabetes-prone (DP) rats are lymphopenic and >80% develop diabetes before 120 days of age (*7, 8*). DR rats were derived from DP progenitors (*9*), have normal lymphocyte numbers and phenotypes, and do not become diabetic spontaneously if maintained in a viral antibody–free (VAF) environment (*10*).

An unexplained outbreak of lymphocytic insulitis (pancreatic islets surrounded and

D. L. Guberski, A. A. Like, J. E. Wallace, R. M. Welsh, Department of Pathology, University of Massachusetts Medical Center, Worcester, MA 01655.
V. A. Thomas, E. S. Handler, A. A. Rossini, Department of Medicine, University of Massachusetts Medical Center, Worcester, MA 01655.
W. R. Shek, Charles River Laboratory, Wilmington, MA 01887.

*To whom correspondence should be addressed.